Tracking shear waves in turbid medium by light: theory, simulation, and experiment

Sinan Li,[1] Yi Cheng,[1] Lipei Song,[2] Robert J. Eckersley,[3] Daniel S. Elson,[2,4] and Meng-Xing Tang[1,*]

[1]*Department of Bioengineering, Imperial College London, London, UK*

[2]*Department of Surgery and Cancer, Imperial College London, London, UK*

[3]*Department of Biomedical Engineering, King's College London, London, UK*

[4]*e-mail: daniel.elson@imperial.ac.uk*

**Corresponding author: mengxing.tang@imperial.ac.uk*

Received August 1, 2013; revised November 6, 2013; accepted February 11, 2014;
posted February 12, 2014 (Doc. ID 195035); published March 12, 2014

Shear wave propagation provides rich information for material mechanical characterization, including elasticity and viscosity. This Letter reports tracking of shear wave propagation in turbid media by laser-speckle-contrast analysis. The theory is described, and a Monte Carlo simulation of light shear wave interaction was developed. Simulation and experiments on tissue-mimicking phantoms agree well and show tracking of shear wave at the phantom surface and at depth as well as multiple shear waves interacting within the object. The relationship between speckle contrast value and shear wave amplitude is also investigated. © 2014 Optical Society of America

OCIS codes: (170.1065) Acousto-optics; (110.0113) Imaging through turbid media.
http://dx.doi.org/10.1364/OL.39.001597

Shear waves are mechanical waves oscillating perpendicular to the propagation direction and have been studied, e.g., in Earth science for understanding the structure of flow of the Earth's mantle [1] as well as in medicine for tissue mechanical characterization. For example, the attenuation and speed of shear waves are related to tissue viscoelastic properties, which in turn provide an indication of the disease state of the tissue. Methods of tracking shear waves propagating at cm scale depth in tissue include the use of ultrasound [2] and magnetic resonance-based methods [3]. Optical observation of tissue response to acoustic radiation force and associated shear wave generation was previously reported in [4,5]. In this Letter, we present a method to track the shear wave propagation in optically turbid media by laser speckle contrast analysis.

Part of our experimental method was discussed in [6], where the shear wave speed was tracked in phantoms of varying elasticity. A coherent green laser was used, and the speckle patterns were received on a CCD camera. Transient shear waves were generated by acoustic radiation force a distance away from laser axis at depth in phantoms. The shear wave was tracked using the time-resolved CCD speckle-contrast difference. In this Letter, we first describe the theoretical basis of this experimental method, then a Monte Carlo simulation system is developed for the first time and verified by experiments. We also show shear wave imaging at the phantom edge using local speckle contrast analysis. In addition, multiple shear waves are simultaneously observed through speckle-contrast detection for the first time, and the relationship between CCD speckle-contrast difference and shear wave amplitude is also studied.

Previous theoretical contributions that explain the interaction of ultrasound and (multiply) scattered light are available in the literature [7–9]. Generally, two mechanisms are thought to be responsible for the ultrasound modulation of light: first, the phase change due to displacement of optical scatterers by ultrasound; second, the phase change due to alteration of the optical refractive index by compression and rarefaction of ultrasound. However, when light interacts with a transient shear wave alone, there are two major differences: (1) the shear wave pressure is small, and therefore little alteration of optical refractive index occurs. As a consequence, the second modulation mechanism may be neglected; (2) the shear wave period is much longer than the ultrasound period and is comparable and most likely longer than the light integration time on the detector. Below we describe a framework that can be used to explain the mechanism of tracking shear waves with CCD speckle-contrast analysis.

A stochastic explanation of CCD speckle analysis was provided [10,11]. The CCD speckle contrast is defined by $C = \sigma/\bar{I}$, where σ and $\bar{I}$ are the standard deviation and the mean of CCD pixel intensities. From first- and second-order statistical analysis and with the assumption of spatial ergodicity, the mean speckle intensity $\bar{I}$, and standard deviation σ are given as [10]

$$\bar{I} = \langle E(t)E^*(t+\tau)\rangle_{t,\varepsilon}|_{(\tau=0)}, \tag{1}$$

$$\sigma = \sqrt{\langle [E(t)E^*(t+\tau)]^2\rangle}_{t,\tau,\varepsilon,}, \tag{2}$$

where E denotes for complex optical field at a CCD pixel, E^* is the conjugate of E. Symbol $\langle\rangle$ denotes for averaging over time t, time derivative τ, and ε, a single realization of the optical scatterer distribution.

Considering an optically turbid medium illuminated with a temporally coherent light, photons can be scattered many times and experience random physical paths before being detected. Therefore, light received at a CCD pixel consists of many such components, and $E(t)$ can be written in a summation form (without consideration of polarization effect for simplicity): $E(t) = \sum_{i=1}^{N} E_j(t)$, in which $E_j(t)$ is one of the many partial components, and N is total number of the partial components. Then

the autocorrelation function of light can be rewritten as $\langle E(t)E^*(t+\tau)\rangle_t = \sum_{i=1}^{N}\sum_{j=1}^{N}\langle E_i(t)E_j^*(t+\tau)\rangle_t$.

For photons traversing the tissue, the optical wavelength is much smaller than the photon-mean free path (hundreds of micrometer in the visible spectrum [12]), and the weak scattering approximation holds. That is to say, photon phase in one scattering path is independent from another, and the phase differences between individual photon paths ($i \neq j$) are uniformly distributed through 0 to 2π, leading to cancellation of the cross terms in $\langle E(t)E^*(t+\tau)\rangle_t$. Then the autocorrelation function of light can be simplified and rearranged as

$$\begin{aligned}\langle E(t)E^*(t+\tau)\rangle_t &= \sum_{i=1}^{N}\langle E_i(t)E_i^*(t+\tau)\rangle_t \\ &= \frac{1}{N}\sum_{i=1}^{N}\left\langle \exp\left[-i\left(\sum_{k=1}^{N'}\Delta\varphi_{ik}(t,\tau)\right)\right]\right\rangle_t,\end{aligned} \tag{3}$$

where $\Delta\varphi_{ik}(t,\tau)$ is the optical phase change in the kth free path of the ith partial wave, which is caused by shear wave modulation of the $(k-1)$th and the kth scatterer displacement during time t to $(t+\tau)$.

The modulation of scatterer displacement results in optical path length changes between two consecutive scatterers. The kth optical free path length can be calculated by

$$\Delta\boldsymbol{r}_{ik}(t) = [\boldsymbol{r}_{ik} + \boldsymbol{u}_{ik}(t)] - [\boldsymbol{r}_{i(k-1)} + \boldsymbol{u}_{i(k-1)}(t)], \tag{4}$$

where $\boldsymbol{r}_{ik}$ and $\boldsymbol{r}_{i(k-1)}$ are the original positions of the kth and the $(k-1)$th scatterer, and $\boldsymbol{u}_{ik}(t)$ and $\boldsymbol{u}_{i(k-1)}(t)$ are the displacements caused by shear wave propagation. Then the optical phase variation can be written as

$$\Delta\varphi_{ik}(t,\tau) = -n\boldsymbol{k}[\Delta\boldsymbol{r}_{ik}(t+\tau) - \Delta\boldsymbol{r}_{ik}(t)], \tag{5}$$

where n is the optical refractive index of the medium, and $\boldsymbol{k}$ is the optical wave number. With Eqs. (3)–(5), the shear wave is connected with the autocorrelation function of light, which, together with Eqs. (1) and (2), can further connect the shear wave field to the CCD speckle statistics. In reality, Brownian motion of scatterers in tissue may also contribute to the autocorrelation function of light. To isolate the shear wave contribution, here we solely consider shear wave modulation in Eq. (4) for conciseness as Brownian motion is an independent process [8].

The shear wave field can be calculated by solving the Navier–Stokes equation. Considering an infinite homogeneous and isotropic viscoelastic medium, an analytical solution is given, utilizing the Green's function formalism in [13]. The shear wave displacement generated by an acoustic radiation force is then deduced with the superposition principle:

$$u(\boldsymbol{r},\tau) = \int \mathrm{d}\tau \iiint f(\boldsymbol{\xi},\tau)g(\boldsymbol{r}-\boldsymbol{\xi},t-\tau)\mathrm{d}\boldsymbol{\xi}, \tag{6}$$

where $f(\boldsymbol{\xi},\tau)$ is the profile of acoustic radiation force in time and space, and $g(\boldsymbol{r},t)$ is the Green's function.

Based on the above theoretical framework, a computer simulation for the optical observation of shear waves was developed. Tissue displacement as a function of time and space due to shear wave propagation was calculated numerically using Eq. (6). The light transport path in tissue displaced by shear wave was predicted by Monte Carlo modeling [14], and, based on the result, we calculate the autocorrelation function of light and time-resolved CCD speckle contrast with Eqs. (3)–(5) and Eqs. (1) and (2). To compute $\Delta\varphi_{ik}(t,\tau)$ in Eq. (3), time is gated consecutively with equal length through exposure time T. Within each gated window, t ranges from 0 to T, τ ranges from 0 to $(T-t)$. Then the auto-correlation function of light can be calculated with time and the time-resolved CCD contrast $C(t)$, or the time-resolved CCD contrast difference $\Delta C(t) = C_b(t) - C(t)$ is obtained, where the background contrast $C_b(t)$ is assumed to be one in simulation.

In the simulation (Fig. 1), a point-like 532 nm laser illuminated a homogeneous sample with an optical absorption coefficient $\mu_a = 0.2\ \mathrm{cm}^{-1}$, optical scattering coefficient $\mu_s = 30\ \mathrm{cm}^{-1}$, anisotropy factor $g = 0.8$, and a reduced scattering coefficient $\mu_s' = 5\ \mathrm{cm}^{-1}$ [15]. The mechanical parameters were set as follows: shear wave speed $c_s = 2.2$ m/s; bulk wave speed $c_p = 1500$ m/s; shear viscosity $\nu_s = 0.1$ Pa. s; and bulk viscosity $\nu_s = 0$ Pa. s [13]. A CCD camera was aligned with the laser to maximize the detected light intensity and positioned sufficiently far from the sample to allow spatial ergodicity to be assumed for speckle statistics. Transient shear waves were generated by the acoustic radiation force, which was perpendicular to the laser axis. This force is constant for 1 ms, and the spatial profile was defined by a simplified ultrasound focus geometry: an ellipse with constant 1 mm lateral and 10 mm axial extent, respectively. The generated shear waves propagate away from the acoustic radiation force.

In the experiment, a tissue-mimicking phantom was made with 0.8% agar in weight and 4% intralipid in volume to achieve similar mechanical and optical parameters to the simulation [6,13,15]. Shear waves were generated by

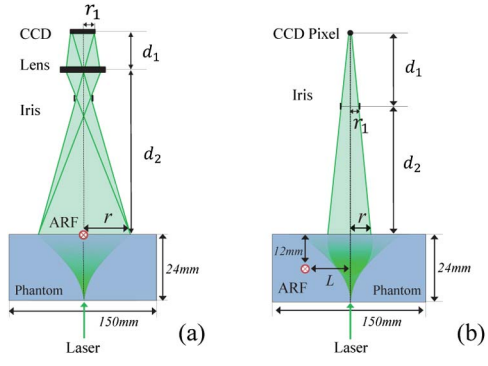

Fig. 1. Schematic of the top view of the simulation/experiment setup. (a) Imaging shear wave front near sample surface: r_1 (3.34 mm) and $r = r_1 d_2/d_1$ are the radii of the imaged CCD array and the projected light exit plane. (b) Tracking shear wave propagating at depth: L (31 mm) is the distance between the laser and the shear wave source; r_1 (3.5 mm) and $r = r_1(d_1 + d_2)/d_1$ are the radii of iris and the CCD pixel projected onto the light exit plane (the single pixel is simplified as a point). ARF denotes for acoustic radiation force, which is loaded in the direction perpendicular to the laser axis.

the transient acoustic radiation force launched by a 1 ms 5 MHz ultrasound burst, and a 1 ms CCD exposure length was used to record the laser speckle patterns. With this configuration, a background contrast $C_b(t) = 0.84$ was achieved without shear waves.

To image shear waves at the sample surface, the acoustic radiation force was aligned with the laser at the light exit plane to generate shear waves. A lens was placed in front of the CCD (1392×1040 pixels) to record the laser speckles at the light exit plane [Fig. 1(a)]. Since shear waves were generated and propagated near the light exit surface, the spatial information carried by the shear wave modulated light was not washed out by multiply scattering. Therefore, the localized CCD speckle contrast was calculated for a kernel size of 15×15 pixels to visualize the shear wave fronts.

When shear waves are generated at depth in the sample, the shear wave modulated light is multiply scattered, and the speckle patterns received at the CCD no longer maintain localized information. Therefore, to track shear waves in bulk media, the acoustic radiation force is applied at a distance from the laser axis [Fig. 1(b)] to observe the shear wave propagation within an optical detection volume (i.e., the volume occupied by the scattered laser beam that is detected by the CCD). In this manner, the laser speckle statistics are affected only by a one-directional shear wave, and the global CCD contrast values calculated over the whole CCD array with time are used to indicate whether the shear wave is within the optical detection volume.

Figures 2(b) and 2(c) show the experimental and simulated results of shear wave imaging of the phantom edge using local speckle contrast difference. For comparison, a simulation of the shear wave displacement in the same plane is shown in Fig. 2(a). The largest CCD contrast difference exists along the shear wave front, where the largest modulation of light due to the shear wave occurred.

To track shear waves at depth, time-resolved CCD contrast curves, rather than an image in Fig. 2, were generated and shown in Fig. 3. As a transient shear wave approaches the optical detection volume, larger numbers of scattered photons fall within the shear wave volume, and thus a larger ratio of light is modulated by the shear wave, causing a reduced CCD contrast C and an increased CCD contrast difference ΔC. The ΔC peaks when the optics and shear wave overlap the most. The time-to-peak in $\Delta C(t)$ indicates the time-of-flight of shear waves, which can be used for shear wave speed measurement. In simulation (solid line in Fig. 3(a)), the peak is shown at 14 ms, agreeing with the preset time-of-flight

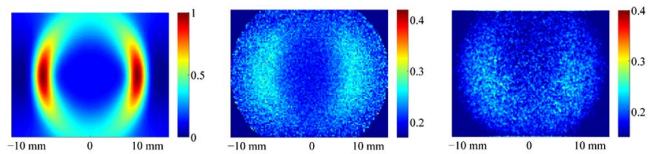

Fig. 2. (a) Simulated near-surface shear wave front with normalized displacement and that imaged by the localized laser speckle contrast difference (ΔC) at 4 ms in (b) simulation and (c) experiment. The acoustic radiation force was launched along the position 0.

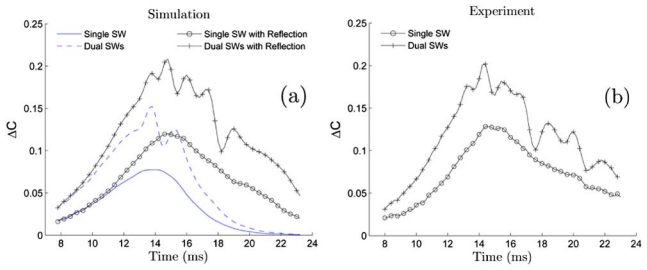

Fig. 3. (a) Simulated and (b) experimental results of time-resolved CCD contrast difference induced by a single shear wave and dual-shear waves at depth. The solid and dashed blue curves in (a) are simulation results without consideration of shear wave reflections; the solid black curves in (a) and in (b) are the simulation and experimental results counted in the shear wave reflections.

($L/c_s = 14$ ms). However, experimental results show the peak value at approximately 15 ms. Further simulation demonstrated that this mismatch was an effect of the shear wave reflection at the phantom boundaries in the experiment (the reflection coefficients of obliquely incident shear waves were calculated based on [16]), which broadened the shear wave and prolonged the measured time-of-flight. Though some reflection bias could exist in real situations, an accurate measurement of shear wave speed can be still obtained by a differential method [6].

As a study of multiple shear waves tracked by the speckle-contrast detection, Fig. 3 also shows the time-resolved CCD contrast difference induced by dual shear waves. Two identical transient shear waves were generated equidistant from the optical axis, propagating toward each other. Results show that, instead of an accumulation of contrast difference induced by each individual shear wave, dual-shear waves generate a pattern in $\Delta C(t)$. With no shear wave reflection, the peak in ΔC is split into two due to dual shear wave interaction over time in the optical detection volume. The "ripples" after the main peaks in experiment are again caused by shear wave reflections from the phantom boundaries and this was confirmed by simulation. The profile of the pattern in time is primarily determined by the mechanical properties of medium and the light distribution in the optical detection volume. With a fixed light distribution, a faster shear wave will result in a more compact pattern due to the reduced shear wave interaction time within the optical detection volume. Also, compared with individual shear waves, multiple shear waves are more sensitive to reflections, which might be useful for geometry characterization.

Figure 4 shows the mapping between CCD contrast difference and the shear wave amplitude. The y axis takes the peak value of $\Delta C(t)$ of the single shear wave in Fig. 3, and the x axis represents the shear wave amplitude. In the simulation, the shear wave amplitude is directly defined as an input by scaling Eq. (6). In the experiment, the varied ultrasound pressures were used to generate shear waves with different amplitudes. As the shear wave amplitude is proportional to the magnitude of the acoustic radiation force, $F = (2\alpha\langle I\rangle)/c$, where c is the ultrasound speed, α is the ultrasound absorption coefficient, and $\langle I\rangle$ is the averaged local ultrasound intensity in time, which

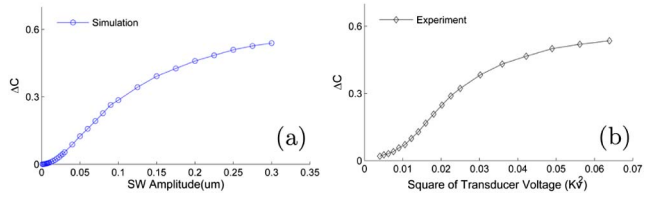

Fig. 4. Peak value of time-resolved CCD contrast difference against shear wave amplitude in (a) simulation and (b) square of transducer input voltage in experiment.

is proportional to the square of transducer input V with an assumption of linear ultrasound prorogation; therefore V^2 is used as the x axis for the experiment to indicate the amplitude of the shear wave. Both simulation and experiment exhibited an S-shaped profile between ΔC and shear wave amplitude. It can be seen that the relationship between CCD contrast difference and shear wave amplitude is not linear over the whole range but can be assumed linear within a smaller range. Figure 4(a) also shows that shear waves with an amplitude of even tens of nanometers may generate a considerable speckle-contrast difference (0.1–0.3), indicating a high sensitivity to shear wave tracking. Generally, Figs. 4(a) and 4(b) agree well despite a larger deviation for large shear wave amplitudes, where higher ultrasound pressures are used and the assumption of linear ultrasound propagation may not hold.

In summary, a theory, simulation, and experiment for tracking shear waves using light and speckle contrast analysis is presented. Compared with ultrasound tracking methods (sensitive to μm displacement), the optical speckle-contrast analysis can be more sensitive because optical wavelengths are a few orders of magnitude smaller than ultrasound wavelengths. The approach could be used in medicine for quantitative elastography by tracking shear waves via time-of-flight [6]. In practice, blood diffusion, Brownian motion, and blood flow will cause speckle decorrelation, and, while this should not affect the time-of-flight estimation, it can reduce the signal-to-noise ratio of the measurements. Additionally, measurements may be cardiac gated to minimize the time-dependent decorrelation. The developed Monte Carlo simulation matches experiments well and could be useful for understanding how $\Delta C(t)$ is related to shear wave properties (e.g., speed and attenuation) and optical configuration (e.g., CCD exposure time). This is the first time, to the best of our knowledge, that shear waves were coupled with coherent light and furthermore related with CCD speckle-contrast statistics in a simulation framework. The simulation will be incorporated with ARF-assisted ultrasound modulated optical tomography [17,18] to study the effect of ARF-generated shear waves on the image resolution. The method can also be generalized to other forms of electromagnetic waves if the speckle patterns can be detected.

The authors thank Prof. David O. Cosgrove for fruitful discussions, and EPSRC (EP/H02316X/1) and the Royal Society for financial support.

References

1. J. Ritsema, H. J. van Heijst, and J. H. Woodhouse, Science **286**, 1925 (1999).
2. K. Nightingale, S. McAleavey, and G. Trahey, Ultrasound Med. Biol. **29**, 1715 (2003).
3. R. Muthupillai, D. Lomas, P. Rossman, J. Greenleaf, A. Manduca, and R. Ehman, Science **269**, 1854 (1995).
4. E. Bossy, A. R. Funke, K. Daoudi, A.-C. Boccara, M. Tanter, and M. Fink, Appl. Phys. Lett. **90**, 174111 (2007).
5. R. J. Zemp, C. Kim, and L. V. Wang, Appl. Opt. **46**, 1615 (2007).
6. Y. Cheng, R. Li, S. Li, C. Dunsby, R. J. Eckersley, D. S. Elson, and M.-X. Tang, Ultrasound Med. Biol. **38**, 1637 (2012).
7. W. Leutz and G. Maret, Phys. B **204**, 14 (1995).
8. L. V. Wang, Phys. Rev. Lett. **87**, 043903 (2001).
9. L. V. Wang, Opt. Lett. **26**, 1191 (2001).
10. R. Zemp, S. Sakadzic, and L. V. Wang, Phys. Rev. E **73**, 061920 (2006).
11. J. Goodman, *Statistical Optics* (Wiley, 1985).
12. W. F. Cheong, S. A. Prahl, and A. J. Welch, IEEE J. Quantum Electron. **26**, 2166 (1990).
13. J. Bercoff, M. Tanter, and M. Fink, IEEE Trans. Ultrason. Ferroelectr. Freq. Control **51**, 396 (2004).
14. L. Wang, S. L. Jacques, and L. Zheng, Comput. Methods Programs Biomed. **47**, 131 (1995).
15. H. J. van Staveren, C. J. M. Moes, J. van Marie, S. A. Prahl, and M. J. C. van Gemert, Appl. Opt. **30**, 4507 (1991).
16. B. A. Auld, *Acoustic Fields and Waves in Solids* (Wiley, 1973).
17. R. Li, L. Song, D. S. Elson, and M.-X. Tang, Opt. Lett. **35**, 2633 (2010).
18. R. Li, D. S. Elson, C. Dunsby, R. Eckersley, and M.-X. Tang, Opt. Express **19**, 7299 (2011).